

University of Massachusetts Dartmouth

Department of Physics

**Turbulently-Driven Detonation Initiation in
Electron-Degenerate Matter with Helium**

A Thesis in

Physics

by

Gabriel Casabona

Submitted in Partial Fulfillment of the

Requirements for the Degree of

Master of Science

August 2019

We approve the thesis of Gabriel Casabona

Date of Signature

Robert Fisher
Associate Professor, Department of Physics
Graduate Program Director, Physics
Thesis Advisor

Gaurav Khanna
Professor, Department of Physics
Thesis Committee

Scott Field
Assistant Professor, Department of Mathematics
Thesis Committee

Jianyi Jay Wang
Chairperson, Department of Physics

Jean VanderGheynst
Dean, College of Engineering

Tesfay Meressi
Associate Provost for Graduate Studies

Abstract

Turbulently-Driven Detonation Initiation in Electron-Degenerate Matter with Helium

by Gabriel Casabona

Type Ia supernovae (SNe Ia) are believed to result from the thermonuclear explosions of carbon-oxygen white dwarfs. While important as standardizable candles, and sources of nuclear enrichment and cosmic rays, the stellar progenitors, as well as the mechanism for detonation of SNe Ia are still unknown. In previous collaborative work, I have shown that a turbulently-driven mechanism can give rise to a detonation in carbon-oxygen electron-degenerate fuel in the distributed burning regime. We have now extended this turbulently-driven detonation mechanism to simulate the detonation of carbon in the presence of helium. Using high-resolution local three-dimensional hydrodynamic simulations with the FLASH4 code, I explore a range of parameter space motivated by leading progenitor models of SNe Ia. I show that the helium abundance greatly affects the range of conditions needed to detonate carbon in electron-degenerate matter. These local models can then be used in subgrid models of nuclear burning and detonation initiation in future global simulations of SNe Ia.

Acknowledgements

This work used the code FLASH 4.0.1, developed by the DOE NNSA-ASC OASCR Flash Center at the University of Chicago. Simulations ran in parallel on the Extreme Science and Engineering Discovery Environment (XSEDE) Stampede2 supercomputer at the University of Texas at Austin's Texas Advanced Computing Center. Plots and analysis of our runs were done with yt. Special thanks to Professor Robert Fisher, for providing the proper guidance in physics and computational techniques to make this work possible and also for providing me with a Research Assistantship. I would also like to thank the Physics department at the University of Massachusetts Dartmouth for their continued support as I advance in my academic career, as well as the university as a whole for providing me with exceptional care to all my needs as a student.

Contents

List of Figures	vi
List of Tables	vii
Chapter 1 Introduction	1
1.1 Type Ia Supernovae	1
1.2 Helium Detonation Models	2
1.3 Turbulence	3
1.4 Distributed Burning Regime	5
1.5 Zel'dovich Gradient Mechanism	5
Chapter 2 Turbulently-Driven Detonation Mechanism	7
2.1 Carbon Detonation	7
2.2 Helium Detonation	8
2.3 Simulation Methodology	8
2.4 Simulation Results	9
2.5 Conclusion	10
References	17

List of Figures

Figure 2.1: Slice plots of temperature and specific nuclear energy generation rate, through the maximum temperature in the z - y plane, for the 512^3 run	13
Figure 2.2: Slice plots of temperature and specific nuclear energy generation rate, for the MinHeLowDen_H run	13
Figure 2.3: Slice plots of temperature and specific nuclear energy generation rate, for the MedHeLowDen_H run	14
Figure 2.4: Slice plots of temperature and specific nuclear energy generation rate, for the PureHeLowDen_H run	14
Figure 2.5: Slice plots of temperature and specific nuclear energy generation rate, for the MinHeHighDen_H run	15
Figure 2.6: Slice plots of temperature and specific nuclear energy generation rate, for the MedHeHighDen_H run	15
Figure 2.7: Slice plots of temperature and specific nuclear energy generation rate, for the PureHeHighDen_H run	16

List of Tables

Table 2.1: A table of carbon-oxygen runs with different resolution, RMS velocity and mean temperature..	7
Table 2.2: A table of helium-carbon-oxygen runs with different resolution, RMS velocity and mean temperature..	12

Chapter 1 Introduction

Type Ia supernovae (SNe Ia) are the thermonuclear explosions of white dwarfs (WDs). These WDs are in binary systems, accreting matter from their companion stars. One of the many unique characteristics of SNe Ia is that they have a consistent peak luminosity, which is why they are used in cosmology as standardizable candles [8]. Their use as standardizable candles helped in the discovery of the accelerated expansion of the universe [9]. SNe Ia are also prominent sources of cosmic rays and the abundance of ^{56}Fe in the universe.

Although it is known that SNe Ia are the thermonuclear explosions of WDs, their detonation mechanism remains unknown. In our previous work [6], we proposed a detonation mechanism for carbon in electron-degenerate matter due to turbulence. Using localized 3-dimensional hydrodynamics simulations, we found that carbon can indeed detonate in electron-degenerate turbulent matter in the distributed burning regime. We refer to this new mechanism as a *turbulently-driven detonation mechanism*. For this project, we explore the parameters of how the detonation of helium may lead to the detonation of carbon. Inspiration comes from previous literature that determined what role the detonation of the helium surface of the WD plays in SNe Ia.

1.1 Type Ia Supernovae

The categorization of SNe begins with hydrogen. Type II SNe are characterized by strong hydrogen absorption lines in their spectrum. SNe II result from the collapse of a massive star, with masses greater than $10 M_{\odot}$, at the end of their lifetime. Type I SNe have no hydrogen lines in their spectra. Furthermore, SNe Ia spectra have strong silicon absorption lines. Early models predicted that SNe Ia must come from a compact object, which was confirmed by SN 2011fe [7]. Astronomers were able to observe the region where the event took place

before and after the explosion, confirming early suspicions. The only two compact objects in the universe that can explode, as far as we know, are WD and neutron stars (NS). NS are known to explode into kilonovae, so strong confidence is put into SN 2011fe originating from a WD.

Progenitors of SNe Ia involve a primary WD in a binary system. In a single-degenerate channel, the secondary is usually a star still on main sequence. Extensive work has gone into exploring single-degenerate models, however, observational evidence does not support this channel since no surviving companion main sequence star has yet been found for a normal SN Ia event.

In the double-degenerate (DD) channel, both the primary and secondary stars are WDs. The primary WD tidally disrupts the secondary WD, creating an accretion disk around the primary. Over time, this disk accretes onto the primary WD, creating a highly turbulent environment. Motivated by the DD channel, our previous work showed that the turbulent cascade caused by the accreting matter can lead to a detonation [6]. Those models included electron-degenerate matter consisting of a 1:1 ratio of carbon and oxygen. For this project, we take this mechanism one step further to explore how turbulence can lead to the detonation of helium, which might then detonate carbon.

1.2 Helium Detonation Models

WD are known to have a relatively thin helium shell around them resulting from stellar evolution [5]. During the merger of these binary systems, the helium of the secondary WD will accrete first and mix with the helium layer of the primary WD. Motivation for this project comes from recent literature which explores various mechanisms of the detonation of this helium layer and how this leads to the detonation of the carbon core. One of these mechanisms is called the double-detonation mechanism. In one possible scenario, two individual spots in the helium layer of the primary WD detonate, sending shock waves radially inwards towards

the carbon core. At the point where the shock waves meet, carbon detonation is initiated at an off-center location.

In a more realistic model, the helium accretion from the secondary WD continuously adds to the helium shell of the primary WD, until the primary detonates [4]. This mechanism adds more kinetic energy since mass is being added into the system with high velocities. Known as the dynamically driven double-degenerate double-detonation, D⁶, SNe Ia are now modeled with a much wider range of initial conditions. An outcome of the D⁶ model is complete detonation of the primary WD, which sends the secondary WD as a hypervelocity runaway. Recent observations from *Gaia* now support the existence of this new model [3], further increasing the need to explore this detonation mechanism.

1.3 Turbulence

The majority of the universe exists in a fluid state, either gas or plasma. For this reason, the study of fluid dynamics is crucial for understanding phenomenon happening in the universe. In astrophysics, modeling fluids takes the form of Euler's equation,

$$\frac{\partial(\rho\mathbf{v})}{\partial t} + \nabla \bullet (\rho\mathbf{v}\mathbf{v}) = -\nabla P - \rho\nabla\Phi,$$

where ρ is the mass density, \mathbf{v} is the velocity vector, P is the thermal pressure, Φ is the gravitational potential, and G is the universal constant of gravitation [2]. In this form, the fluid has zero viscosity and includes effects from self-gravity. This project involves modeling electron-degenerate matter at scales much higher than those needed to have viscosity play a role, so the approximation of the Euler fluid will suffice.

In the simplest of cases, fluids are modeled as a laminar flow. This means that the velocity vector lines are all smoothly varying. Realistic cases, however, need to include turbulence, in which the velocity vector lines are no longer smooth. This is caused from chaotic changes

in the fluid's velocity and pressure. The onset of turbulence typically begins with some kind of fluid instability. Rayleigh-Taylor and Kelvin-Helmholtz are two of the major instabilities found in astrophysics.

An important quantity that is needed when describing turbulence is the dimensionless Reynold's number, (Re), defined as

$$\text{Re} = \frac{\rho u L}{\mu}.$$

Here, ρ is the density of the fluid, u is the velocity of the fluid, L is the linear dimension, and μ is the dynamic viscosity of the fluid. Re above 2000 means that the fluid flow becomes turbulent. Astrophysical fluids have low viscosities, resulting in them almost always being turbulent. An important quantity here is the linear dimension, meaning that the Re number is dependent on the length scales in question, a property which will be exploited later.

One important aspect of turbulent flow is the onset of a turbulent cascade. Kolmogorov's theory of turbulence tells us that the turbulent cascade allows for the cascade of energy. When turbulence is first initiated, its eddies are at the largest length scales, which is determined by the geometry of the system. The time-scale of these eddies is determined by its turnover time, the time it takes for one eddy to make one complete loop. As time evolves, these eddies break up and form smaller ones, which then have smaller time-scales. Once this time-scale is small enough, the viscosity of the fluid then dissipates the kinetic energy of the turbulence into heat. In our previous work, we showed that when the time-scale of the eddies reduces even lower until equaling that of the nuclear burning time-scale, this is the moment of the initiation of detonation [6]. Another important aspect of Kolmogorov's theory is that the turbulence becomes isotropic as the time-scales are reduced, for high Re numbers. This means that regardless of the large scale eddies, which is determined by the geometry of the system, the statistics of initial range turbulence are universal.

1.4 Distributed Burning Regime

In a regime with negligible turbulence, the nuclear burning is laminar. This flame is characterized by a length, l , and a speed, s_l . The flame maintains a well-defined structure since turbulence has little effect on it. When turbulence begins to influence the structure of the flame, we then consider the dimensionless Karlovitz number, (Ka), defined as

$$\text{Ka} = \sqrt{\frac{v_{\text{RMS}}^3 l}{s_l^3 L}},$$

where L is the integral scale and v_{RMS} is the RMS velocity at the integral scale. When $\text{Ka} < 1$, turbulence is low enough that the structure of flame remains intact. For $\text{Ka} > 1$, turbulence begins to disrupt the structure of the flame. For $\text{Ka} \gg 1$, the flame is completely disrupted by the turbulence. The flame now exists in the distributed regime, where the turbulent mixing dominates electron conduction. In regions of key interest in the double-degenerate channel of SNe Ia, $\text{Ka} \simeq 10^4$, deep into the distributed burning regime, another motivator of this project.

1.5 Zel'dovich Gradient Mechanism

To better understand the significance of the distributed burning regime, it is important to note what the leading theory was in detonation mechanisms for SNe Ia. First modeled by Zel'dovich and collaborators [10], the Zel'dovich gradient mechanism describes how a laminar flame may lead to a detonation. It begins with the formation of a laminar flame in a hot background, accelerating down a temperature gradient. The formation of the flame initiates a shock front ahead of it. If the temperature gradient is shallow enough, then this initially subsonic laminar flame will accelerate just behind the shock front. The shock front leading the flame front allows for the carbon in that regime to fully burn, causing a detonation.

When the temperature is too steep, the shock front will accelerate much quicker than the flame front, leaving it behind. In this case, carbon is not fully burned, causing a failed detonation. Failed detonations with the Zel'dovich gradient mechanism put a lower limit on the temperatures needed to detonate carbon. Our previous work shows with turbulence taken into consideration, critical temperatures for carbon detonation are a factor of 2-3 times lower than previous studies based upon Zel'dovich.

Chapter 2 Turbulently-Driven Detonation Mechanism

2.1 Carbon Detonation

In our previous work, we determined that our turbulently-driven detonation mechanism can lead to the detonation of carbon in electron-degenerate matter. Three-dimensional hydrodynamic simulations were carried out with electron-degenerate fuel consisting of equal ratios of carbon and oxygen in a density of 10^7 g cm^{-3} . Through extensive statistical tests, detonation initiation occurred when the time scale of the turbulence, characterized by the eddy-turnover time on the critical length scale, becomes larger than the nuclear burning timescale, $t_{edd}/t_{burn} \simeq 10^9$.

Table 2.1: Results from initial work that established a turbulently-driven detonation mechanism using only carbon and oxygen. Mass-weighted mean temperature at the time of detonation in each resolution are listed.

Resolution	T_{mean} (K)
64^3	1.12×10^9
128^3	1.17×10^9
256^3	1.17×10^9
512^3	1.18×10^9

An important implication of these runs is that detonation of carbon can occur in the distributed burning regime through our turbulence mechanism. This is especially important since the Zel'dovich gradient mechanism has been the leading mechanism explaining spontaneous detonation initiation in SNe Ia. Although not wrong, it lacks the physics of turbulence

which we know must play a role in the DD channel. From these results, we can now utilize our new mechanism to explore other parameters within these mergers.

2.2 Helium Detonation

Having now a successful detonation mechanism, incorporating helium is a natural next step. As explained before, the detonation of the helium layer of the primary WD opens up the parameter space of how the carbon core can be detonated. Previous work done by Holcomb and collaborators determined tight constraints with regards to temperature, density, and critical length scales for helium burning based upon the Zel'dovich gradient mechanism [1]. They performed one-dimensional hydrodynamic simulations with various initial conditions similar to that which can be modeled with SNe Ia progenitor models. With a turbulently-driven detonation mechanism, we now can perform three-dimensional hydrodynamic simulations and explore the constraints previously modeled.

2.3 Simulation Methodology

Computational tools were used to analyze the physics of turbulence. FLASH, a multiphysics multiscale code built for high-energy density physics, was used to execute three-dimensional hydrodynamic simulations. The hydrodynamics solver used in this case was the split piecewise parabolic method (PPM). The Helmholtz equation of state was used to incorporate the contributions from nuclei, electrons, blackbody photons, electron-degeneracy, and relativistic effects [11]. Since this work is only considering a small number of nuclear species, a 19-isotope network was used [12], [13].

In all, 18 simulations were conducted. Each one had a domain size of $L = 100$ km, simulated in a fully-periodic box. Spatial resolution ranged from 128^3 (L), 256^3 (M), and 512^3 (H) cells, on a uniform grid. Within each resolution, the parameter space of density and nuclear composition was explored. Densities were set to 10^5 (LowDen) and 10^6 (HighDen)

g cm^{-3} . Initial helium abundance varied from 100% (PureHe), 25% (MedHe), and 10% (MinHe). Carbon and oxygen took up the remaining portion with an assumed equal ratio to one another for each simulation. Initial temperature in all simulations began at 10^8 K .

Simulations begin with all the fluid having zero velocity. A large-scale stochastic forcing routine is then used as a stirring mechanism to increase the momentum of the simulation. Each simulation runs until the RMS velocities reach a stable value, indicating that it has reached steady-state turbulence. At this point, the simulations are restarted with nuclear burning turned on and are continued to determine whether detonation will occur. Detonation was classified as the time where helium abundance dropped by 10% of initial value.

2.4 Simulation Results

Slice plots were generated for temperature and specific nuclear burning using the highest resolution models, 512^3 . A snap shot is taken at the time when the detonation has initiated, with the box centered about the point of maximum temperature, which, owing to the extreme sensitivity of the rates to temperature, is also the point of maximum nuclear burning. At this angle, one is looking through the x -axis on the z - y plane. Each slice plot has an inset which is zoomed in on the hotspot.

Figure 2.2 shows the slice plots for the MinHeLowDen_H run, which has a $v_{\text{rms}} = 1.26 \times 10^8 \text{ cm s}^{-1}$. For all resolutions, these runs fully detonated helium but saw an increase in carbon abundance, while keeping oxygen almost steady. This implies that the helium was burnt off through the triple-alpha process into carbon. Carbon abundances showed no signs of coming to a detonation.

Figure 2.3 shows the slice plots for the MedHeLowDen_H run, which has a $v_{\text{rms}} = 1.28 \times 10^8 \text{ cm s}^{-1}$. Similar to the previous set of parameters, these runs also saw complete detonation of helium with an increase in carbon, while keeping oxygen steady. This also

implies that the triple-alpha process fused most of the helium into carbon, while showing no signs of a carbon detonation.

Figure 2.4 shows the slice plots for the PureHeLowDen_H run. None of these runs, at all resolutions, detonated. However, helium is seen to also burn into carbon through the triple-alpha process. The slice plots are of the last time step recorded, which has a $v_{\text{rms}} = 1.25 \times 10^8 \text{ cm s}^{-1}$. A detonation may be observed if simulations ran long enough but this will be explored in more detail in future work.

Figure 2.5 shows the slice plots for the MinHeHighDen_H run, which has a $v_{\text{rms}} = 1.22 \times 10^8 \text{ cm s}^{-1}$. All resolutions of these runs saw a detonation of helium and then of carbon shortly afterwards. They also see a rise in oxygen, which implies that on top of the traditional triple-alpha process occurring, an additional alpha capture on carbon occurs to fuse into oxygen.

Figure 2.6 shows the slice plots for the MedHeHighDen_H run, which has a $v_{\text{rms}} = 5.82 \times 10^7 \text{ cm s}^{-1}$. These runs also show complete detonation of helium and carbon with some formation of oxygen, with indications that heavier elements must have been formed post-detonation.

Figure 2.7 shows the slice plots for the PureHeHighDen_H run, which has a $v_{\text{rms}} = 1.25 \times 10^8 \text{ cm s}^{-1}$. These runs see an almost full detonation of helium, with the abundance ratio falling sharply from 100% to 20%. At the onset of detonation, carbon abundance rises from 0% to near 17.5%, then immediately fully detonates. Oxygen remains steadily at 0%, indicating again that heavier elements have been formed.

2.5 Conclusion

This body of work confirms that turbulently-driven detonation can occur with various abundance levels of helium, carbon, and oxygen. More specifically, the critical temperature for carbon detonation is robustly a factor of $\sim 2 - 3$ times lower than theorized from previous

studies based upon Zel'dovich. Opening up the parameter space of initial conditions for possible detonation scenarios has been an ongoing endeavour for many decades. With newer observational datasets such as *Gaia*, we can now put constraints on our models and also put our focus on specific channels that match these observations. Further work includes exploring more abundance ratios, higher resolutions, and incorporating more in-depth species networks that would allow us to better understand the nucleosynthesis in these simulations.

Table 2.2: A table of runs with the different resolutions, densities, helium abundances, and mean temperature at the time of detonation initiation, T_{det} (K).

Resolution	Density (g cm ⁻³)	Helium Abundance	T_{det} (K)
128^3	10^5	0.1	8.22×10^8
128^3	10^5	0.25	8.77×10^8
128^3	10^5	1.0	None
128^3	10^6	0.1	7.80×10^8
128^3	10^6	0.25	7.87×10^8
128^3	10^6	1.0	9.91×10^8
256^3	10^5	0.1	8.25×10^8
256^3	10^5	0.25	8.83×10^8
256^3	10^5	1.0	None
256^3	10^6	0.1	7.99×10^8
256^3	10^6	0.25	8.81×10^8
256^3	10^6	1.0	1.09×10^9
512^3	10^5	0.1	8.28×10^8
512^3	10^5	0.25	8.75×10^8
512^3	10^5	1.0	None
512^3	10^6	0.1	7.80×10^8
512^3	10^6	0.25	6.30×10^8
512^3	10^6	1.0	1.06×10^9

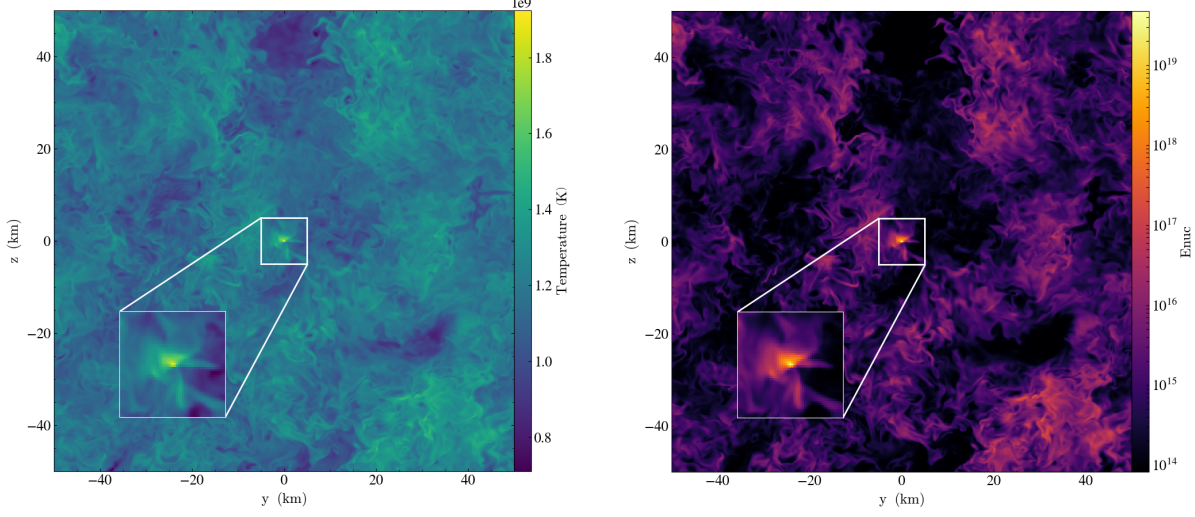


Figure 2.1: Slice plots of temperature and specific nuclear energy generation rate from the C/O run, through the x-axis in the z - y plane, for the 512^3 . Each is centered about the hot spot just before leading into a detonation.

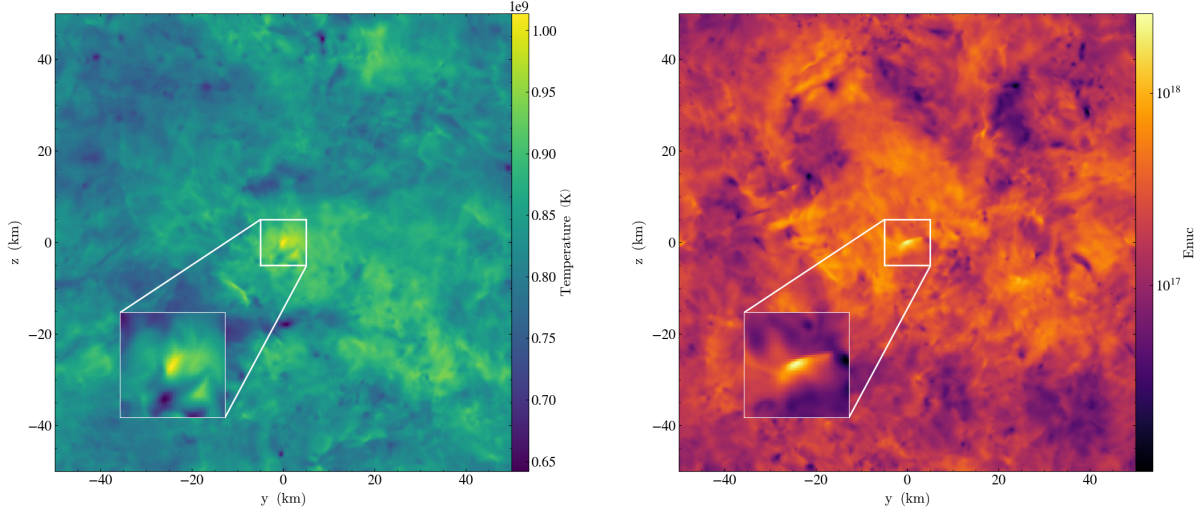


Figure 2.2: Slice plots of temperature and specific nuclear energy generation rate, for the MinHeLowDen_H run, through the x-axis in the z - y plane, at the onset of detonation.

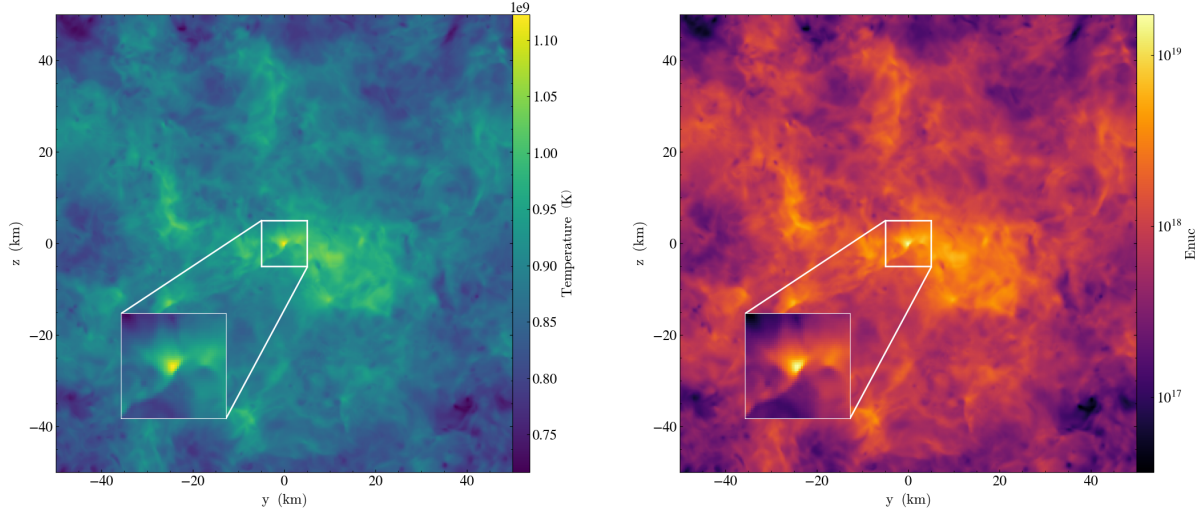


Figure 2.3: Slice plots of temperature and specific nuclear energy generation rate, for the MedHeLowDen_H run, through the x-axis in the z - y plane, at the onset of detonation.

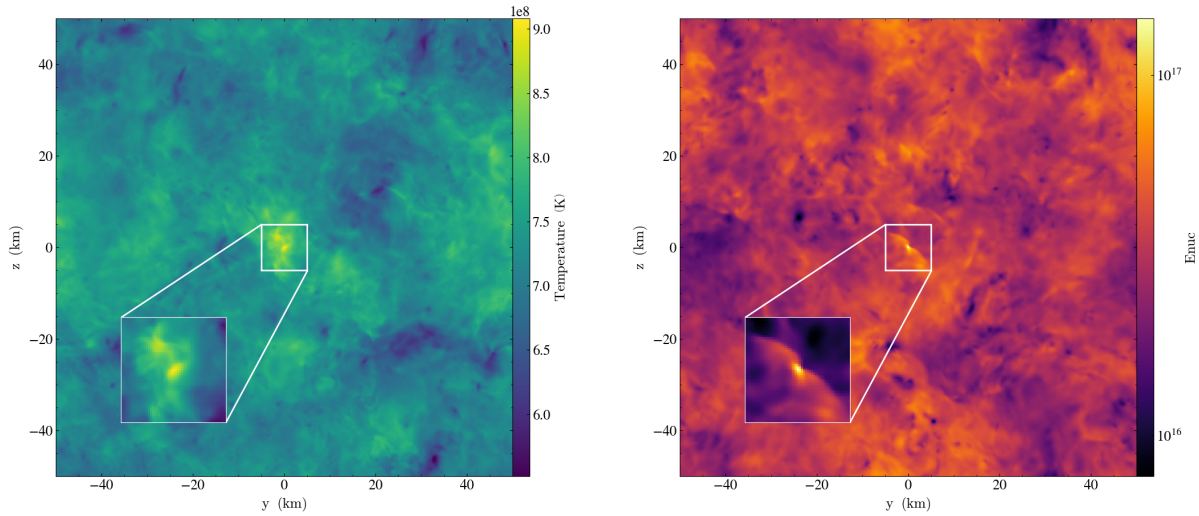


Figure 2.4: Slice plots of temperature and specific nuclear energy generation rate for the PureHeLowDen_H run, through the x-axis in the z - y plane, at the last time step of the run.

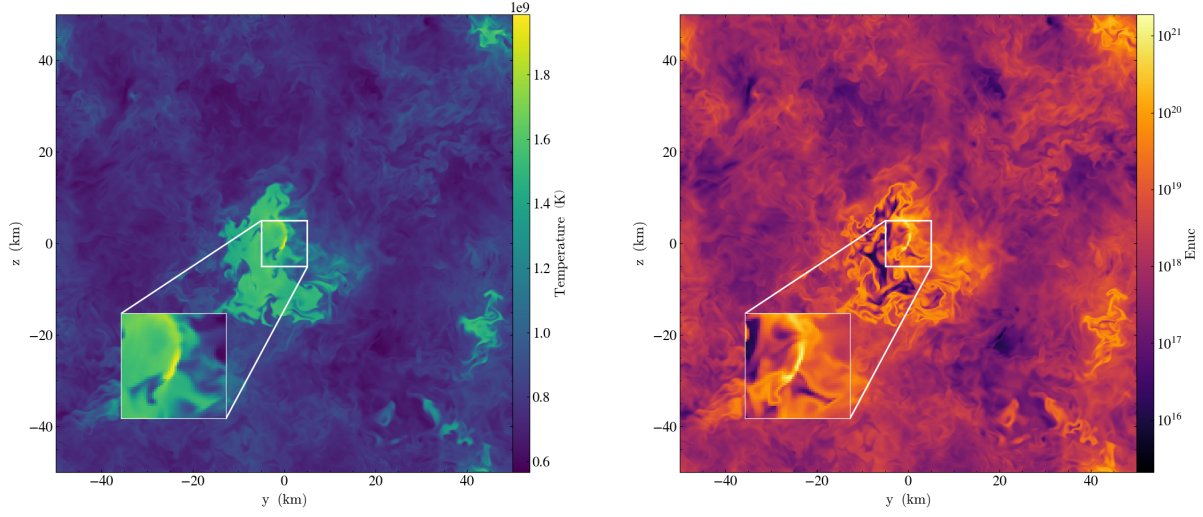


Figure 2.5: Slice plots of temperature and specific nuclear energy generation rate, for the MinHeHighDen_H run, through the x-axis in the z - y plane, at the onset of detonation.

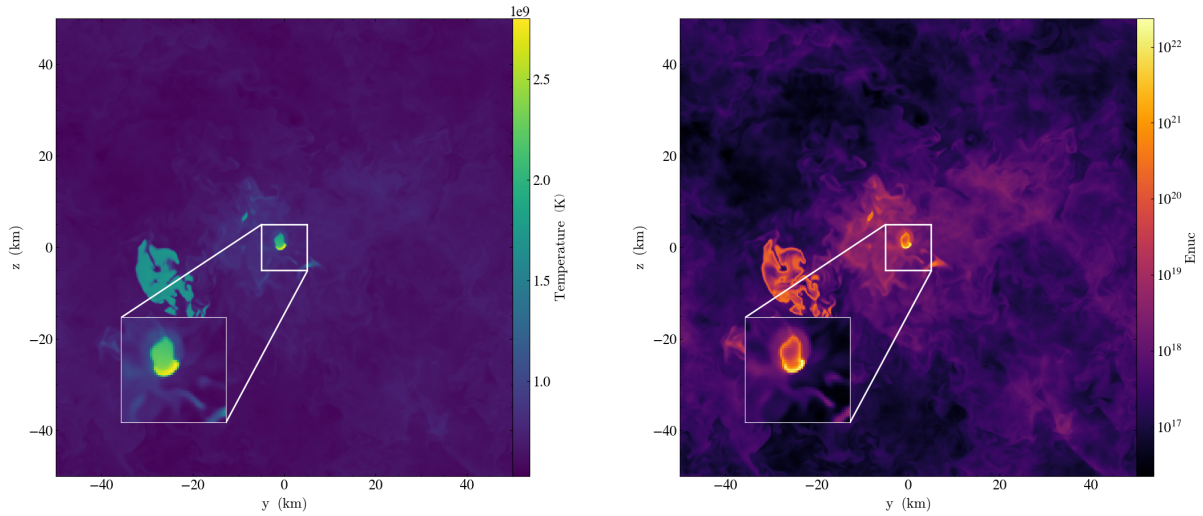


Figure 2.6: Slice plots of temperature and specific nuclear energy generation rate, for the MedHeHighDen_H run, through the x-axis in the z - y plane, at the onset of detonation.

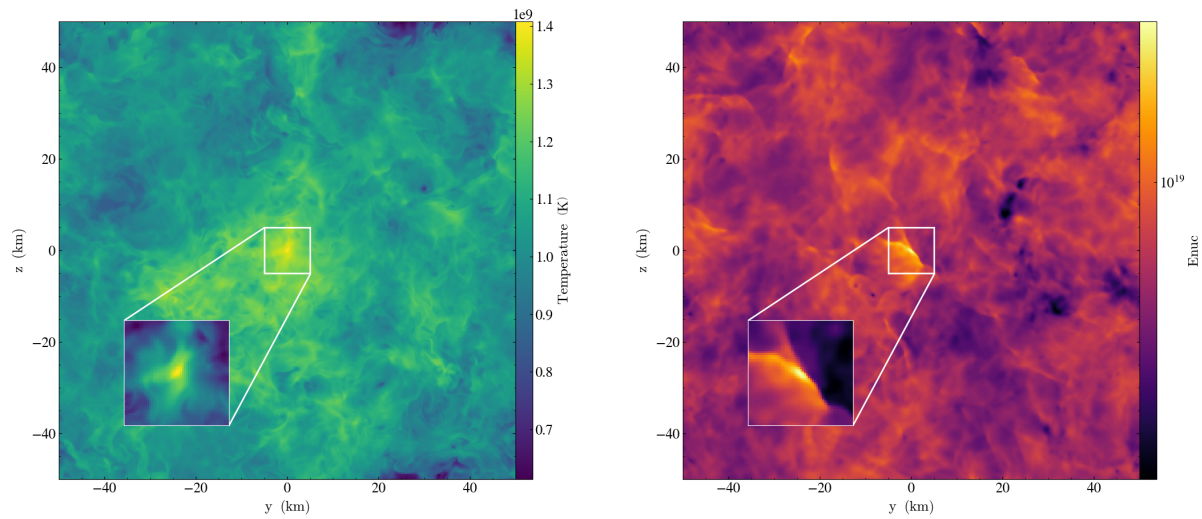


Figure 2.7: Slice plots of temperature and specific nuclear energy generation rate, for the PureHeHighDen_H run, through the x-axis in the z - y plane, at the onset of detonation.

References

- [1] C. Holcomb *et al*, Astrophysical Journal **771**, 14 (2013).
- [2] J.K. Truelove *et al*, Astrophysical Journal **495**, 821 (1998).
- [3] K. Shen *et al*, Astrophysical Journal **865**, 14 (2018).
- [4] K. Shen *et al*, Astrophysical Journal **854**, 15 (2018).
- [5] N. Giannicchele *et al.*, Nature **554**, 73 (2018).
- [6] R. Fisher *et al.*, Astrophysical Journal **876**, 64 (2019).
- [7] P. E. Nugent *et al.*, Nature **480**, 344 (2011).
- [8] M. M. Phillips, Astrophysical Journal Letters **413**, L105 (1993).
- [9] Riess *et al.*, Astrophysical Journal **116**, 1009 (1998).
- [10] Y. B. Zel'dovich *et al.*, Journal of Applied Mechanics and Technical Physics **11**, 264 (1970).
- [11] F. X. Timmes and S. E. Woosley, Astrophys. J. **396**, 649 (1992).
- [12] T. A. Weaver *et al.*, Astrophys. J. 225, 1021 (1978).
- [13] F. X. Timmes, Astrophysical Journal Supplement **124**, 241 (1999).